Cold Shock Domain of the Human Y-Box Protein YB-1. Backbone Dynamics and Equilibrium between the Native State and a Partially Unfolded State†

Cathelijne P. A. M. Kloks, Marco Tessari, Geerten W. Vuister, and Cornelis W. Hilbers*

NSRIM Centre, Faculty of Science, University of Nijmegen, Toernooiveld 1, 6525 ED Nijmegen, The Netherlands

Received March 10, 2004; Revised Manuscript Received June 5, 2004

ABSTRACT: The three-dimensional structure of the central cold shock domain (CSD) of the human Y-box protein (YB-1 CSD) is virtually identical to those available for the bacterial cold shock proteins (Csp's). We have further characterized YB-1 CSD by studying its dynamics by nuclear magnetic resonance. The observed structural similarity is reflected in the backbone dynamics, which for YB-1 CSD is very similar to that of the *Escherichia coli* protein CspA. The rotational correlation time of YB-1 CSD shows that it is a monomer. This indicates that the dimerization observed for the YB-1 protein is not caused by its CSD, but involves other parts of this protein. The YB-1 CSD is only marginally stable as are the mesophilic bacterial Csp's. In contrast to the rapid two-state folding of the bacterial Csp's, the formation of the native form of YB-1 CSD is slow and at least a three-state process. The NMR experiments revealed the presence of a second state of YB-1 CSD in equilibrium with the native form. The exchange rates from and to the folded state are in the order of 0.2 and 0.5 s^{-1}, respectively. Relaxation experiments indicated that the second state is a highly flexible, partly structured molecule.

NMR relaxation measurements have gained a prominent position in studies of the internal mobility of biomacromolecules (*1*, *2*). The high spectral resolution of the modern NMR spectrometers combined with multidimensional heteronuclear techniques allows investigation of the relaxation behavior of individual atoms or groups of atoms in biomacromolecules and thereby yields an unprecedented detailed picture of the dynamics of such molecules. The frequencies of the internal motions (including conformational changes) may vary considerably, i.e., from motions occurring in the second and millisecond up to the picosecond time scale. NMR relaxation experiments can be used to characterize these phenomena, although different NMR approaches are often required to determine the motions in the different frequency regions. Most frequently, ^{15}N-T_1, ^{15}N-T_2, and heteronuclear NOE ({^{1}H-^{15}N}-NOE) experiments have been used to characterize the motion of the N−H^N amide groups of the protein backbone.

Current approaches used to interpret the results of such measurements are the so-called model-free approach (*3*, *4*) and the (reduced) spectral density mapping method (*5*−*9*). The first method characterizes the internal motion in terms of an order parameter S^2, which is a measure of the freedom of motion of a single atom or a group of atoms in a molecule. The second method provides the values of the spectral densities of the internal motions of an atom or a group of atoms at their respective Larmor frequencies. Exchange phenomena, as for example the exchange between different local conformational sites, are also reflected in the relaxation parameters. A particular form of conformational exchange, the transition between the folded and unfolded state of proteins, has so far received limited attention. The mixture of signals arising from the different forms complicate the spectrum interpretation and often result in increased spectral overlap, which makes relaxation studies inherently more difficult. A well-known example is the N-terminal SH3 domain of the protein drk (drkN SH3), which exists in equilibrium between a folded and unfolded state in aqueous solution (*10*, *11*). Two other examples are the 131 residue-fragment of staphylococcal nuclease, Δ131Δ (*12*, *13*), and the peripheral subunit-binding domain of pyruvate dehydrogenase multienzyme complex (*14*).

In this article, we describe the backbone dynamics of the cold shock domain (CSD), which is the central, nucleic acid binding domain of the human Y-box protein, YB-1. Y-box proteins are involved in transcriptional and translational regulation. The general domain structure of this class of proteins is presented in Figure 1a, together with the consensus sequence of their CSDs. Previously, we derived the three-dimensional structure of the YB-1 CSD (*15*). The core of this domain consists of a five-stranded, antiparallel β-barrel (Figure 1b,c) exhibiting a folding pattern characteristic of the oligonucleotide/oligosaccharide binding-fold (OB-fold) protein family (*16*). Just like drkN SH3, the folded form of YB-1 CSD coexists in a dynamic equilibrium with a second form, which we prove here to be largely unstructured. This form is referred to as the unfolded form indicated with U in the remainder of this article. We investigate the relaxation properties of these two forms and characterize their exchange properties. The results are compared with those of bacterial cold shock proteins (Csp's) for which the three-dimensional

† This research was supported by The Netherlands Foundation for Chemical Sciences with financial assistance from The Netherlands Organization for Scientific Research (NOW).

* To whom correspondence should be addressed: Phone +31-24-3652160. FAX: +31-24-3652112. E-mail: ceesh@sci.kun.nl.

10.1021/bi049524s CCC: $27.50
Published on Web 07/14/2004

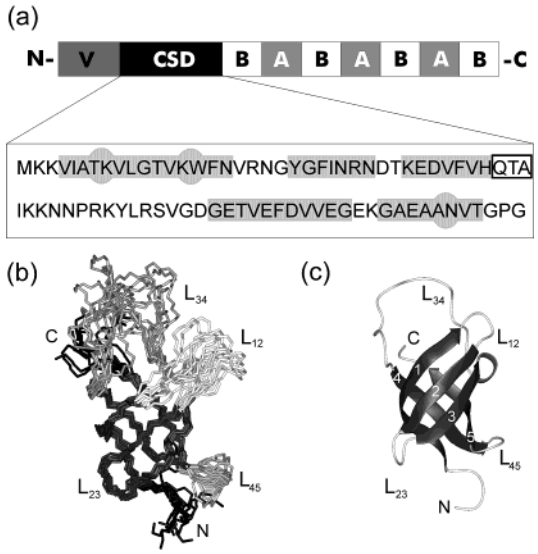

FIGURE 1: (a) General domain structure of the Y-box proteins. V is the variable N-terminal domain, CSD is the cold shock domain, B and A are the 30 amino acids-long basic and acidic blocks forming the C-terminal domain. Below this, the sequence of the CSD is presented including the position of the β-strands (gray boxes), β-bulges (gray ovals), and the 3^{10}-helix (boxed). (b) Structure ensemble of the CSD (pdb file 1h95) with different shading for the two termini and the loops connecting the β-strands. (c) Ribbon diagram representation of the first structure of the ensemble depicted in panel b. The numbering of the β-strands is indicated in white. The structures in b and c were produced by means of the program MOLMOL 2.6 (*39*).

structure and dynamics are also known. The backbone dynamics of YB-1 CSD and *Escherichia coli* CspA protein are very much alike showing that the close similarity of their structures also translates into similar dynamical properties. The formation of the native structures of YB-1 CSD and the bacterial Csp's appears, however, very different. The apparent rate of formation of YB-1 CSD has diminished by 3 orders of magnitude compared to that of the Csp's. Moreover, the folding of the YB-1 CSD involves at least a three-state process, while the bacterial Csp's exhibit effectively two-state folding.

MATERIALS AND METHODS

Samples. Uniformly ^{15}N-labeled CSD samples were prepared as described by Kloks et al. (*17*). The NMR samples consisted of 0.5−1.5 mM protein (79 residues, molecular weight 8740 Da) in 250 μL of 95% H_2O/5% D_2O at pH 6.7 in Shigemi tubes.

NMR Experiments. The NMR experiments were performed at 298 K, on a Bruker DRX spectrometer operating at 600 MHz (14.1 T), and on Varian UnityInova spectrometers operating at 500 and 750 MHz (11.7 and 17.6 T, respectively). Spectra were processed using NMRPipe (*18*) and assigned using PIPP (*19*). The relaxation experiments were analyzed using the NMRDraw and NlinLS programs of the NMRPipe package.

Resonances of the unfolded state were assigned with the aid of a ^{15}N-ROESY−HMQC experiment using a mixing time of 34 ms and with a ^{15}N-HMQC−NOESY−HSQC experiment. Furthermore, the suite of experiments, used in the analysis of the folded state (*15*, *17*), was also used to complete the assignment of the unfolded state.

^{15}N-$T_{1\rho}$ and ^{15}N-T_1 experiments were recorded at 11.7 and 17.6 T. Furthermore, a {^{1}H-^{15}N}-NOE experiment was performed at 11.7 T. The spectra were recorded in 3-fold, for different relaxation periods, in an interleaved fashion to check for reproducibility and were co-added before analysis. The $T_{1\rho}$ values were corrected for the T_1 contributions originating from the frequency offset. To access the effect of the exchange between the folded and the unfolded state on the relaxation parameters, an HSQC-exchange experiment (*20*) and a T_1-exchange experiment (*21*) were performed at 11.7 and 17.6 T, respectively. In addition, a ^{15}N-HSQC was recorded of YB-1 CSD at 6 M guanidinium chloride.

Data Analysis. In the presence of exchange between a folded and unfolded state, the longitudinal relaxation (T_1) can be described in general by the following expressions based on the Bloch equations (*21* and references therein):

$$\frac{dM_{zF}}{dt} = -R_{1F}(M_{zF} - M_{zF}^0) + k_{UF}M_{zU} - k_{FU}M_{zF} \quad (1)$$

$$\frac{dM_{zU}}{dt} = -R_{1U}(M_{zU} - M_{zU}^0) + k_{FU}M_{zF} - k_{UF}M_{zU} \quad (2)$$

with solutions:

$$M_{zF}(t) = \frac{M_{zF}(0)}{\lambda_1 - \lambda_2}\{[-(R_{1F} + k_{FU} + \lambda_2)e^{\lambda_1 t} + (R_{1F} + k_{FU} + \lambda_1)e^{\lambda_2 t}] + k_{FU}[e^{\lambda_1 t} - e^{\lambda_2 t}]\} \quad (3)$$

and

$$M_{zU}(t) = \frac{M_{zU}(0)}{\lambda_1 - \lambda_2}\{[-(R_{1U} + k_{UF} + \lambda_2)e^{\lambda_1 t} + (R_{1U} + k_{UF} + \lambda_1)e^{\lambda_2 t}] + k_{UF}(e^{\lambda_1 t} - e^{\lambda_2 t})\} \quad (4)$$

The subscripts U and F refer to the folded and unfolded form; in the derivation a two-state equilibrium has been assumed between U and F. $M_{zU}(t)$ and $M_{zF}(t)$ represent the magnetization as a function of time, and $M_{zU}(0)$ and $M_{zF}(0)$ are the initial magnetization at the start of the relaxation period of the unfolded and folded forms, respectively. M_{zU}^0 and M_{zF}^0 are the corresponding equilibrium magnetizations. The longitudinal relaxation rate constants of U and F are denoted by $R_{1U} = 1/T_{1U}$ and $R_{1F} = 1/T_{1F}$, respectively. Furthermore, k_{UF} and k_{FU} are the exchange rate constants for the transition from the unfolded to the folded and from the folded to the unfolded state, respectively. In addition, λ_1 and λ_2 are given by:

$$\lambda_{1,2} = \Big[-(R_{1F} + k_{FU} + R_{1U} + k_{UF}) \pm \sqrt{\{(R_{1F} + k_{FU}) - (R_{1U} + k_{UF})\}^2 + 4k_{FU}k_{UF}}\Big]/2 \quad (5)$$

To simplify analysis, the T_1-exchange experiment as described by Farrow et al. (*21*) can be used. This experiment enables the direct observation of exchange cross-peaks that reflect the conversion between the folded and unfolded state. The time dependence of the intensity of these cross-peaks corresponds to the last term of eqs 3 and 4. The expressions for the time evolution of the auto- and exchange cross-peak intensities observed in a T_1-exchange experiment

(*10*, *21*) are highly analogous to the corresponding terms in eqs 3 and 4:

$$M_{FF}(t) = \frac{M_F(0)}{\lambda_1 - \lambda_2}[-(R_{1F} + k_{FU} + \lambda_2)e^{\lambda_1 t} + (R_{1F} + k_{FU} + \lambda_1)e^{\lambda_2 t}] \quad (6)$$

$$M_{UU}(t) = \frac{M_U(0)}{\lambda_1 - \lambda_2}[-(R_{1U} + k_{UF} + \lambda_2)e^{\lambda_1 t} + (R_{1U} + k_{UF} + \lambda_1)e^{\lambda_2 t}] \quad (7)$$

$$M_{FU}(t) = \frac{k_{FU}M_F(0)}{\lambda_1 - \lambda_2}(e^{\lambda_1 t} - e^{\lambda_2 t}) \quad (8)$$

$$M_{UF}(t) = \frac{k_{UF}M_U(0)}{\lambda_1 - \lambda_2}(e^{\lambda_1 t} - e^{\lambda_2 t}) \quad (9)$$

Here, $M_{FF}(t)$ and $M_{UU}(t)$ represent the magnetization giving rise to the auto-peaks while $M_{FU}(t)$ and $M_{UF}(t)$ give rise to the exchange cross-peaks. $M_F(0)$ and $M_U(0)$ denote the initial longitudinal magnetization of the folded and unfolded state, respectively, at the start of the relaxation period. The T_1-exchange experiment requires data analysis of both the auto- and exchange cross-peaks. The overlap and the relatively low signal-to-noise ratio of these peaks impose a significant restriction on the number of residues that could be examined and on the precision of the derived parameters. In fact, only nine residues of YB-1 CSD were amenable to such an analysis (vide infra). For short relaxation periods, the relaxation and exchange rates can be accessed directly by simplifying eqs 6−9 with an initial slope approximation:

$$M_{FF}(t) = -M_F(0)(R_{1F} + k_{FU})t + M_F(0) \quad (10)$$

$$M_{UU}(t) = -M_U(0)(R_{1U} + k_{UF})t + M_U(0) \quad (11)$$

$$M_{FU}(t) = k_{FU}M_F(0)t \quad (12)$$

$$M_{UF}(t) = k_{UF}M_U(0)t \quad (13)$$

To access the internal dynamics of the folded and unfolded state of YB-1 CSD, conventional T_1 and $T_{1\rho}$ experiments were used. These experiments suffer less from the limited signal-to-noise ratio and spectral overlap than the T_1-exchange experiment.

For the two-state equilibrium considered, the decay curves of the conventional T_1 experiment are generally biexponential, as described by eqs 3 and 4. In our case, however, the experimental points are very well fitted with a monoexponential curve. As shown in Appendix I, at these conditions the experimental relaxation rate is determined by the rate constants R_{1F} or R_{1U}.

Just as for the T_1 experiment, monoexponential fitting of the data is justified for $T_{1\rho}$. The exchange rate is small compared to the transverse relaxation rates. Taken the experimental accuracy into account, we can use the standard expressions for the $T_{1\rho}$ decay, with $R_{1\rho}$ equal to $1/T_{1\rho}$.

The intensities of the NOE cross-peaks can be influenced by the exchange between the folded and unfolded state. In the case of exchange, the ratio of the peak intensities of the ^{15}N-magnetization of the folded and unfolded state in the presence and absence of proton saturation, I_{Fz}(sat) and I_{Fz}(unsat), respectively (*10*), can be described by the following expression:

$$\frac{I_{Fz}(\text{sat})}{I_{Fz}(\text{unsat})} = \frac{\{R_{1F} + \sigma_F(\gamma_H/\gamma_N) + \alpha[R_{1U} + \sigma_U(\gamma_H/\gamma_N)]\}}{R_{1F} + k_{FU} - \alpha k_{UF}} \quad (14)$$

Here, σ_F and σ_U are the ^{1}H-^{15}N cross-relaxation rates in the folded and unfolded form, respectively. The constant α is given by $k_{FU}/(R_{1U} + k_{UF})$, and the γ_H and γ_N denote the gyromagnetic ratios of ^{1}H and ^{15}N. Given the values derived for the exchange rates, it can be shown that for the folded state the effect of the exchange is negligible since α is on average 0.1. In this case, eq 14 reduces to the standard expression for the steady-state Overhauser effect. For the NOEs of the unfolded form, an expression similar to eq 14 can be derived, but the relative magnitude of the exchange and relaxation rates prohibited the application of the simplifications.

The relaxation data obtained at 11.7 T were analyzed using reduced spectral density mapping (*5*−*9*) using a home-written script.

RESULTS

Assignment. The CSD consists of 79 residues. In solution, the folded form (F) and largely unfolded form (U) coexist in a ratio of about 70 to 30%, respectively, as determined from their relative peak intensities. In previous papers (*15*, *17*), 67 out of 77 backbone amide ^{1}H and ^{15}N resonances had been assigned for the folded state. The complete resonance assignment of the folded domain as well as scalar couplings and relaxation times has been added to the BioMagResBank entry with accession number 4147.

In the present work, the spectrum interpretation was extended with the assignment of the backbone amide ^{1}H and ^{15}N resonances originating from unfolded form of the protein using a ^{15}N-HSQC experiment (see Figure 2), a ^{15}N-ROESY−HMQC experiment and a ^{15}N-HMQC−NOESY−HSQC experiment. The resonance positions of the side chains of the unfolded domain were identified using the three-dimensional experiments mentioned in Kloks et al. (*15*). In total 225 resonances of the backbone and side chains of the unfolded form could be identified, although not all could be assigned to particular residues, e.g., in the region ^{1}H(7.9−8.5 ppm) − ^{15}N(119−126 ppm) in Figure 2. For some residues, more than one unfolded form seems to be present (see Figure 2). For freshly prepared samples, the signal intensity of these additional unfolded forms is relatively low, and the presence of these forms will not be considered in the remainder of this paper. Over longer time periods, i.e., half a year or more, the intensity ratios of these peaks change and also aggregation of the protein occurs. In some cases, even in freshly prepared samples, the intensity of the second unfolded conformer may be significant, e.g., for U11, U42, and U74. These residues were not incorporated in the analysis of the kinetics of the folding−unfolding process of YB-1 CSD, because no exchange peaks between folded and unfolded forms could be observed in the T_1-exchange experiment. Several reasons, which are not always clear, may be responsible for the absence of these exchange peaks, but

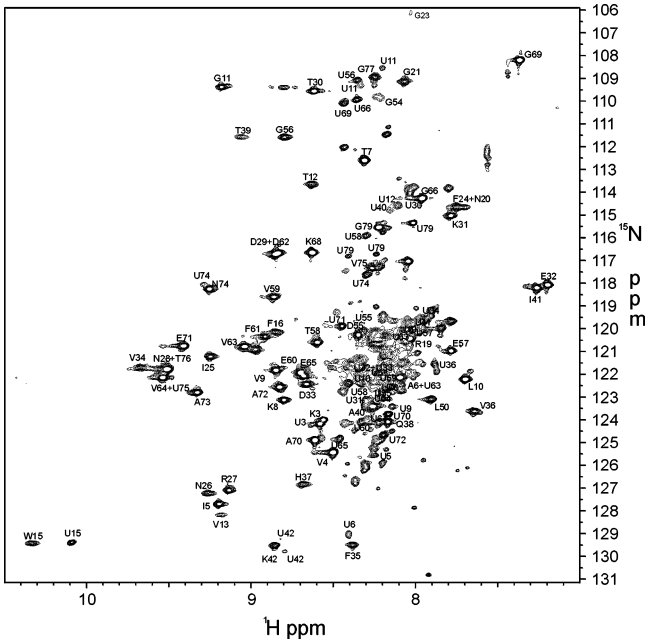

FIGURE 2: The ^{15}N-HSQC spectrum of YB-1 CSD. The peaks from the residues of the folded state are annotated with the one-letter code for amino acids, while the peaks belonging to the unfolded state are labeled with "U".

for residue 42 this is probably due to conformational exchange in the unfolded form (vide infra). The chemical shifts and relaxation data of the unfolded state have been submitted to the BioMagResBank entry under accession number 5076.

A comparison of the assigned signals of the unfolded state and signals in the ^{15}N-HSQC spectrum of YB-1 CSD dissolved in a 6 M guanidinium chloride solution (data not shown) shows that many of the resonances of the unfolded form are outside the region characteristic of a random coil protein indicating the presence of residual structure in the unfolded state U.

Relaxation and Exchange Parameters. Before elaborating on the dynamics of YB-1 CSD, we start by assessing the exchange rates from and to the folded and unfolded state. In the T_1-exchange spectrum, the ^{1}H-^{15}N amide auto- and exchange cross-peaks of nine residues are amenable to an exchange analysis (see Materials and Methods). A section of the spectrum containing the auto- and cross-peaks of glycine 66 is shown in the right panel of Figure 3. We determined the initial slopes of the decay curves of M_{FF} and M_{UU} as well as that of the build-up curve of the exchange cross-peaks to obtain values for $R_{1F} + k_{FU}$, $R_{1U} + k_{UF}$, k_{FU} and k_{UF} (cf. eqs 10−13) from which the values of R_{1F} and R_{1U} could be estimated (left panel in Figure 3 and Table 1). The magnitude of the k_{FU} and k_{UF} values (0.2 and 0.5 s^{-1}, respectively) indicates that the exchange between the folded and unfolded form is slow compared to the rates observed for the bacterial Csp's (vide infra).

From this experiment and from the peak intensities in the HSQC spectrum, the equilibrium constant for the folding transition, K_F (= k_{UF}/k_{FU}), was determined at 25 °C and pH = 6.7 (cf. Table 1 and Figure 4). The values derived from the initial slope analysis of the T_1-exchange spectrum have relatively large error bars because of the low intensity of the exchange cross-peaks but are within experimental

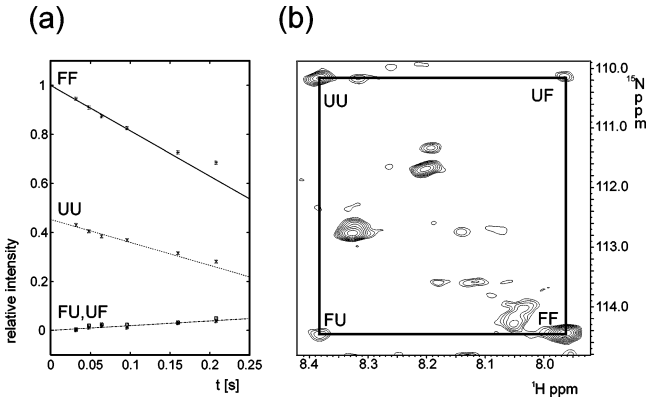

FIGURE 3: Right panel: Section of the T_1-exchange spectrum of YB-1 CSD showing the four resonances (connected by horizontal and vertical bars) belonging to Gly^{66}, i.e., the auto-peaks FF and UU and the cross-peaks UF and FU. Left panel: Fit of the initial slopes of the time-dependent intensity of the four peaks of Gly^{66} in the T_1-exchange spectrum.

Table 1: Relaxation and Exchange Parameters Derived for YB-1 CSD from the T_1-Exchange Experiment Conducted at 17.6 T[a]

residue	R_{1F} [s^{-1}]	R_{1U} [s^{-1}]	k_{FU} [s^{-1}]	k_{UF} [s^{-1}]
5	1.3 ± 0.2	2.0 ± 0.3	0.3 ± 0.05	0.9 ± 0.2
6	1.6 ± 0.2	2.2 ± 0.3	0.1 ± 0.05	0.4 ± 0.1
31	1.8 ± 0.2	1.5 ± 0.3	0.2 ± 0.05	0.7 ± 0.2
32	1.9 ± 0.2	1.9 ± 0.3	0.2 ± 0.05	0.5 ± 0.1
41	1.7 ± 0.2	2.2 ± 0.3	0.2 ± 0.05	0.5 ± 0.1
66	1.6 ± 0.1	1.6 ± 0.3	0.2 ± 0.05	0.4 ± 0.1
69	1.4 ± 0.1	2.1 ± 0.3	0.2 ± 0.05	0.4 ± 0.1
70	1.5 ± 0.1	2.1 ± 0.2	0.2 ± 0.05	0.3 ± 0.05
71	1.6 ± 0.2	1.9 ± 0.2	0.3 ± 0.05	0.3 ± 0.05

[a] R_{1F}, R_{1U}, k_{FU}, and k_{UF} have been determined using an initial slope approximation.

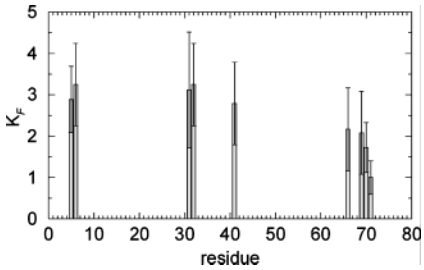

FIGURE 4: The folding constants, K_F, of YB-1 CSD as a function of residue number, calculated from the cross-peak intensities in the HSQC spectrum and from the (k_{UF}/k_{FU}) ratio of the T_1-exchange experiment.

accuracy equal to those obtained from the HSQC spectrum. The K_F values cluster around a value 2.5, which indicates that the exchange behavior of the residues in YB-1 CSD reflects the same process.

Since nine residues are not sufficient to describe the backbone dynamics of a protein, conventional relaxation experiments were used to obtain an estimate of the internal backbone flexibility of the two states of YB-1 CSD. Equations 3 and 4 suggest that the T_1-relaxation curves be biexponential, but biexponential fitting of the results proved to be unjustified statistically. Instead the experimental curves could be well fitted with a monoexponential function. At such conditions the effective relaxation rates represent the rate constants R_{1F} and R_{1U} (see Appendix I). The relaxation parameters derived from these experiments, R_{1F}, R_{1U}, $1/T_{1\rho F}$, and $1/T_{1\rho U}$, and the heteronuclear NOE are summarized in

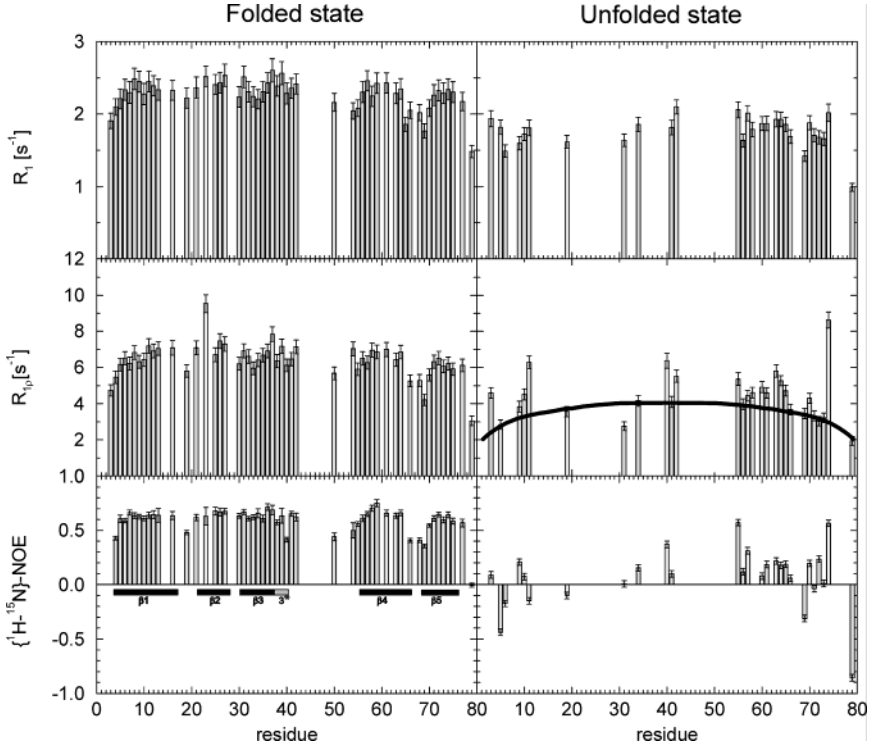

FIGURE 5: The relaxation rates R_1, $R_{1\rho}$, and $\{^1H\text{-}^{15}N\}$-NOE for the folded and unfolded state of YB-1 CSD recorded at 11.7 T. The secondary structure elements are shown in the panel in the left lower corner. The drawn line in the $R_{1\rho}$ panel of the unfolded state indicates the theoretical $R_{1\rho}$ values of a random coil (see text).

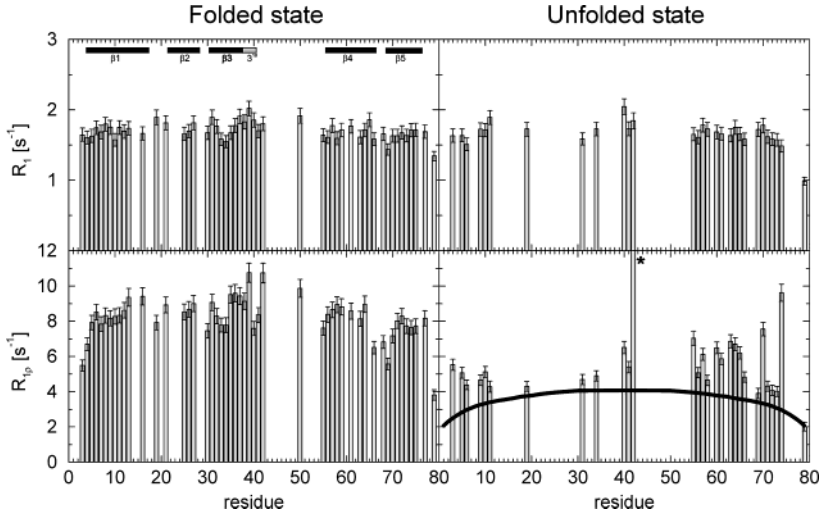

FIGURE 6: The relaxation rates R_1, $R_{1\rho}$ for the folded and unfolded state of YB-1 CSD recorded at 17.6 T. Residue 42 of the unfolded state, marked with the asterisk, has an $R_{1\rho}$ of 14.3 ± 1.0 s^{-1}. The secondary structure elements are shown in the panel in the left upper corner. The drawn line in the $R_{1\rho}$ panel of the unfolded state indicates the theoretical $R_{1\rho}$ values of a random coil (see text).

Figures 5 and 6 and for the nine residues in Tables 2 and 3. Using the ratio between ρ_F and $T_{1\rho F}$ values (*22*), we estimated the rotation correlation time, τ_c, of the folded state of YB-1 CSD to be equal to 4.9 ns. Within the error margin, there is a good correspondence between the value of R_{1F} derived from the conventional experiment ($R_{1F\ \text{classical}}$, Table 2) and that from the T_1-exchange experiment (R_{1F}, Table 1), both recorded at 17.6 T. The agreement for the R_{1U} values is less good, but in view of the accuracy of the data acceptable.

Comparison of the data of the conventional T_1 experiments in Table 3 and Figure 5 with those in Table 1 and 2 and Figure 6 shows that at 11.7 T, the R_{1F} values have increased systematically with respect to the values obtained at 17.6 T. The ratio $R_{1F}(17.6\ \text{T})/R_{1F}(11.6\ \text{T}) \cong 0.78$, which is in good agreement with the value expected for a globular protein with a rotational correlation time of 4.9 ns. The transverse relaxation rates increase when proceeding from 11.7 to 17.6 T and the ratio $R_{1\rho F}(17.6\ \text{T})/R_{1\rho F}(11.6\ \text{T}) \cong 1.22$ again is in good agreement with the value expected for the given correlation time. On the other hand, for the unfolded form the T_1-relaxation times for these two field strengths are virtually equal, i.e., $R_{1U}(17.6\ \text{T})/R_{1U}(11.7\ \text{T}) \cong 1$. We notice that $R_{1U}(11.7\ \text{T})$ is smaller than $R_{1F}(11.7\ \text{T})$, but that $R_{1U}(17.6\ \text{T})$ is equal to $R_{1F}(17.6\ \text{T})$. The $R_{1\rho U}$ values, however, exhibit a more conventional behavior in that they increase with increasing field strengths.

The T_1, $T_{1\rho}$, and NOE data collected at 11.7 T were used to calculate the spectral density of the different residues of

Table 2: Longitudinal and Transverse Relaxation Rates of Nine Residues of YB-1 CSD at 17.6 T Using Either Conventional Experiments (R_{1F} Classical, R_{1U} Classical) or the T_1-Exchange Experiments ($R_{1\rho F}$ and $R_{1\rho U}$)[a]

residue	$R_{1F\ classical}$ [s^{-1}]	$R_{1U\ classical}$ [s^{-1}]	$R_{1\rho F}$ [s^{-1}]	$R_{1\rho U}$ [s^{-1}]
5	1.5 ± 0.1	1.6 ± 0.1	7.9 ± 0.4	5.1 ± 0.3
6	1.8 ± 0.1	1.5 ± 0.1	8.5 ± 0.4	4.4 ± 0.3
31	1.8 ± 0.1	1.6 ± 0.1	9.1 ± 0.5	4.7 ± 0.3
32	1.8 ± 0.1		8.3 ± 0.4	
41	1.7 ± 0.1	1.7 ± 0.1	8.4 ± 0.4	5.4 ± 0.3
66	1.6 ± 0.1	1.6 ± 0.1	6.5 ± 0.4	4.8 ± 0.3
69	1.4 ± 0.1	1.7 ± 0.1	5.6 ± 0.3	3.9 ± 0.3
70	1.6 ± 0.1	1.8 ± 0.1	7.2 ± 0.4	7.6 ± 0.4
71	1.6 ± 0.1	1.6 ± 0.1	8.0 ± 0.4	4.3 ± 0.3

[a] See text.

Table 3: Longitudinal and Transverse Relaxation Rates of Nine Residues of YB-1 CSD at 11.7 T Using Either Conventional Experiments (R_{1F} Classical, R_{1U} Classical) or the T_1-Exchange Experiments ($R_{1\rho F}$ and $R_{1\rho U}$)[a]

residue	$R_{1F\ classical}$ [s^{-1}]	$R_{1U\ classical}$ [s^{-1}]	$R_{1\rho F}$ [s^{-1}]	$R_{1\rho U}$ [s^{-1}]
5	2.2 ± 0.1	1.8 ± 0.1	6.2 ± 0.4	2.8 ± 0.3
6	2.3 ± 0.1	1.5 ± 0.1	6.5 ± 0.4	
31	2.5 ± 0.1	1.6 ± 0.1	6.9 ± 0.4	2.8 ± 0.2
32	2.3 ± 0.1		6.6 ± 0.4	
41	2.4 ± 0.1	1.8 ± 0.1	6.5 ± 0.4	4.1 ± 0.3
66	2.1 ± 0.1	1.7 ± 0.1	5.3 ± 0.3	3.7 ± 0.3
69	1.8 ± 0.1	1.4 ± 0.1	4.2 ± 0.3	3.5 ± 0.3
70	2.1 ± 0.1	1.9 ± 0.1	5.6 ± 0.3	4.3 ± 0.3
71	2.3 ± 0.1	1.7 ± 0.1	6.3 ± 0.4	3.3 ± 0.3

[a] See text.

the folded form (see Figure 7) and will be discussed in the next paragraph.

DISCUSSION

Dynamics of the Folded State. The folded state of YB-1 CSD has a rotation correlation time, $\tau_c = 4.9$ ns, typical of a 9-kDa protein, which shows that the CSD is monomeric. Y-box proteins have been reported to be involved in multiple cellular functions through nucleic acid binding and multimerization. This is also true for the YB-1 protein, which binds to DNA and RNA. It was also demonstrated that the protein might form homodimers in vitro and in vivo (*23*). The finding that under NMR solution conditions the CSD is monomeric suggests that other parts of the protein than the CSD are responsible for this process.

The conventional relaxation data of the folded state of YB-1 CSD (Figures 5 and 6), and the spectral densities derived from these (Figure 7) lead to a flexibility pattern of the backbone, which is similar to that observed for many other proteins. A comparison of the results obtained for YB-1 CSD and CspA of *E. coli* (*24*) is particularly interesting. The backbone dynamics of these two proteins show a striking resemblance. The only difference is that L_{12} of CspA seems to exhibit more conformational exchange, but the paucity of data available for L_{12} in YB-1 CSD makes a detailed comparison very difficult. In all, not only do the folded forms of the two polypeptides have the same topology, but they also have very similar dynamical properties.

Residues of loops L_{12} and L_{45} are involved in DNA binding, and the somewhat enhanced flexibility of these loops, compared to the core of the protein, facilitates complex formation, particularly in situations where nonspecific interaction is concerned, because it allows the protein to adjust its conformation to variations in the sequence of the target DNA.

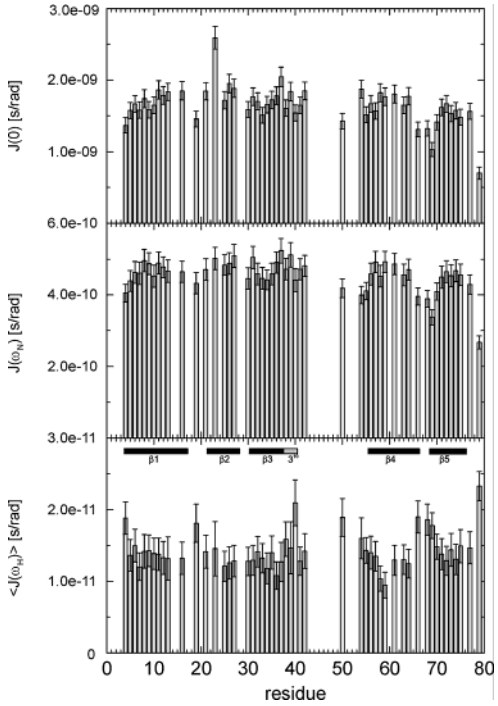

FIGURE 7: Spectral densities obtained from the relaxation data of YB-1 CSD determined at 11.7 T as a function of residue number (see text). The spectral densities at zero-frequency, nitrogen frequency and the average proton frequency are shown. In the lowest panel, the secondary structure elements are indicated.

Enhanced flexibility is also observed for Ala^{40} and Leu^{50}. Ala^{40} is the last residue of the small 3^{10}-helix at the beginning of the large loop L_{34}, and Leu^{50} is the only residue in this loop that shows detectable signals. Flexibility and possible exchange of the amide protons cause the lack of signals from this part of the molecule. The fact that the Leu^{50} signals can be observed even though it is located in the middle of the loop may be explained by the observation that in the OB-fold family, to which YB-1 CSD belongs, loop L_{34} contains a hydrophobic plug that fills the cavity along the long axis of the barrel (*16*). In CspA, this plug is Leu^{45} (*24*), and in YB-1 CSD, the Leu^{50} is a likely candidate. The (weak) hydrophobic interactions with the core may be the reason underlying the diminished flexibility of the backbone amide group of Leu^{50} compared to the remainder of the loop. At this point, we can neither explain this observation due to the lack of NOEs from Leu^{50} to the core, nor its functional significance.

The data obtained for some residues indicate the presence of local conformational exchange. This is clear for the N- and C-terminal regions, as observed oftentimes for other proteins (cf. Figure 5). It is also outspoken for Gly^{23}. This residue is located in the β2-strand of the β-hairpin formed by strands β1 and β2. Its $R_{1\rho}$ value at 11.7 T is significantly larger than that of the other residues, while at 17.6 T its resonance has broadened beyond detection. The same conclusion follows from the examination of the spectral density plots. Thus, $J(0)$ of Gly^{23} is significantly higher than the average value obtained for the whole molecule, while $<J(\omega_H)>$ of Gly^{23} is close to the average value. These observations indicate that this residue monitors or is subjected

to a conformational exchange process in the millisecond time region. Most likely, it is the first process that is responsible. Opposite of Gly[23], in the β-hairpin, we find Phe[16] and given the room provided by the glycine residue, the phenylalanine ring will stack upon the β-sheet as seen in related proteins (*25*). The ring will, however, be free to rotate between stacked states inducing the exchange effects observed for Gly[23]. Finally, spectral density results (Figure 7) suggest a somewhat increased flexibility, in nanosecond regime, for the residues of the loops L_{12}, and L_{45}. Most of the signals of the large loop, L_{34}, are not seen in the spectrum except that of the remarkable residue Leu[50] almost in the middle of that loop. This residue also shows a somewhat increased flexibility in the nanosecond regime compared to the core of the YB-1 CSD.

Flexibility in the Unfolded Form. The flexibility of the backbone of the unfolded form is grossly different from the folded form as indicated by the {^{1}H-^{15}N}-NOE and $T_{1\rho}$ data.

The combination of the relatively low ratio between R_{1U} measured at 17.6 and at 11.7 T and values of the heteronuclear NOE between 0.2 and 0.6 as found in some parts of the molecule (see Figures 5 and 6) only occurs when motions on the nanosecond time scale are present (*26*). This provides a qualitative indication that these parts of the molecule are tumbling with a rate representative of residual structure. Also the transverse relaxation times are indicative of such behavior. This follows from a comparison of the $T_{1\rho}$ data with relaxation rates predicted for a completely random coil protein. The latter rates can be calculated based on the following simple model in which the $R_{1\rho}$ of residue i ($R_{1\rho,i}$) in the sequence of a protein with unrestricted segmental motion depends on its position as follows (*27*):

$$R_{1\rho,i} = R_{\text{intrinsic}} \sum_{j}^{N} e^{-|i-j|/\lambda_0} \qquad (15)$$

$R_{\text{intrinsic}}$ features the intrinsic relaxation rate and depends on the viscosity and temperature of the solution. N is the total number of residues of the chain, and λ_0 is the persistence length (in number of residues). Thus, the relaxation of residue i does not so much depend on the identity of its neighbors but predominantly on the motional properties of the chain. In our calculations, we chose $\lambda_0 = 7$ as found earlier (*27*). Then the result for the completed denatured protein is $R_{\text{intrinsic}} = 0.27\ s^{-1}$, which is reasonably close to the value found for lysozyme (*27*, *28*). A bold line in Figures 5 and 6 indicates the results, obtained at 11.7 and 17.6 T. Several residues, in particular, in the C-terminal region have larger $R_{1\rho}$ relaxation rates than seen for the random coil molecule, indicating the presence of nonrandom structure. The available data are not sufficient to define the structure of the unfolded state further, although one might speculate that the β-hairpin formed by the C-terminal end in the folded structure still is present in the unfolded form.

The conclusions are supported by a comparison of the ^{15}N-HSQC spectrum of the unfolded form with that of the protein dissolved in a 6 M guanidinium chloride solution (data not shown). Several resonances, which in the spectrum of the unfolded form were still close to the positions of the folded form, now have to random coil positions. This was particularly clear for residues 6, 11, 42, 74, and 75, indicating that these residues are part of regions with residual structure supporting, the interpretation of the NOE and $R_{1\rho}$ measurements. These residual structures should not be looked upon as rigid entities as is illustrated by the behavior of Lys[42]. Its $R_{1\rho}$ value increases by a factor of ≈ 2 when proceeding from 11.7 to 17.6 T as a result of a strong line broadening of the cross-peak. This corresponds to conformational exchange, which is fast on the NMR time scale. Because such an effect was not seen for the Lys[42] signal of the folded state it can be attributed to exchange within the residual structure of the unfolded form and does not reflect the transition from the unfolded to the folded state. A similar result, although not as pronounced, is obtained for Ala[70].

Folding and Unfolding of YB-1 CSD Differs from that of the Topologically Equivalent Bacterial Csp's. The folding−unfolding behavior of the bacterial Csp's has been studied extensively. This includes the proteins CspA from the mesophilic bacterium *E. coli* (Ec) (*29*, *30*), CspB from the mesophilic *Bacillus subtilis* (Bs) (*31*), the Csp proteins from the thermophilic bacterium *B. caldolyticus* (Bc) (*30*, *31*), and hyperthermophilic bacterium *Thermotoga maritima* (Tm) (*31*). These bacterial molecules are representative of the class of single-domain proteins that fold and unfold in an all-or-none process without populating "long-living" structured intermediates. Their folding reactions are fast and of the same order of magnitude, i.e., k_{UF} is $\approx 700\ s^{-1}$ at 25 °C, despite their different stabilities. This difference is apparent in their unfolding rates (*31*, *32*). For the mesophilic Bs-CspB and thermophilic Bc-Csp the difference in stability could be traced to the mutation of only two surface residues, i.e., Glu[3] in the mesophilic protein is converted to an arginine residue in the thermophilic protein and likewise Glu[66] into a leucine residue. This occurs despite the fact that the two proteins differ in sequence at 10 additional positions (*33*).

YB-1 CSD exhibits an equilibrium between 70% folded and 30% unfolded state in contrast to the Csps. This is corroborated by the doubling of the resonances observed in the ^{15}N-HSQC spectrum of YB-1 CSD (Figure 2), a phenomenon not seen in the spectra of Ec-CspA (*24*), CspB (34), and Tm-Csp (*35*). In line with this result, the conversion from the unfolded state of YB-1 CSD to the native state is clearly much slower (3 orders of magnitude) than the transition of the denatured to folded state observed for the bacterial Csp's. The result is surprising, because the structure of the YB-1 domain very closely resembles that of the Csp's (*15*). Before elaborating on this point, we note that the exchange cross-peaks observed in the T_1-exchange spectra of the CSD were tacitly assumed to stem from the direct conversion of the unfolded into folded form and vice versa. In fact, this approach implies that the unfolded form observed for YB-1 CSD is a productive, on-pathway folding intermediate, involved in the reaction:

$$\mathbf{D} \underset{k_{DU}}{\overset{k_{UD}}{\rightleftharpoons}} \mathbf{U} \underset{k_{UF}}{\overset{k_{FU}}{\rightleftharpoons}} \mathbf{F} \quad \text{(on-pathway)}$$

Here D is the denatured, random coil protein, U is the observed, unfolded form with residual structure, and F is the native, folded form. However, we cannot a priori exclude that more complicated schemes prevail, for instance, that the unfolded form is a misfolded state that must completely unfold before the native state can be formed, as found in

the so-called off-pathway situation characterized by the reaction:

$$\mathbf{U} \underset{k_{UD}}{\overset{k_{DU}}{\rightleftharpoons}} \mathbf{D} \underset{k_{DF}}{\overset{k_{FD}}{\rightleftharpoons}} \mathbf{F} \quad \text{(off-pathway)}$$

In this situation, the formation of the native state, F, from the completely unfolded state, D, might still exhibit the folding characteristics found for the bacterial Csp's, i.e., a folding rate $k_{DF} \approx 700\ s^{-1}$ and an unfolding rate $k_{FD} \approx 10\ s^{-1}$ (similar to that of the mesophilic proteins). It is important to be able to decide whether such a situation obtains, because this would still leave room for the interesting possibility that CSD molecules might all fold with similar formation rates. In Appendix II, we show that only at some very specific conditions the observed k_{FU} values can be reconciled with the kinetics of the mesophilic bacterial CSD protein. Although, we cannot formally exclude this situation, there is no a priori reason that such conditions are applicable to our protein and we consider it unlikely to occur. In line with current ideas in which protein folding takes place by traversing a free-energy surface from the random coil form to the native folded state, we think more complicated schemes than the simple on and off-pathway reactions, e.g., parallel pathways, are dictating the conversion between these states.

From the extensive studies on the prokaryotic Csp's, alluded to above, it appears, that these proteins have identical topologies and very nativelike and similar transition states. These states are reached late in the folding process. The native state stabilities of the proteins vary, but not according to the folding rates, which are virtually constant. The differences in the stabilities are reflected in the unfolding rates, suggesting that interactions formed in the conversion from the transition state to the native state are responsible for the differential stabilities (*36*). The elegant comparative study on the mesophilic Bs-CspB and the thermophilic Bc-Csp (*33*) presents a nice example of this point of view. It indicates that the interactions of two surface residues, Arg^3 and Leu^{66}, in Bc-Csp are formed in the last step of the native state formation.

On the other hand, it is well known that the rate-determining barrier in the folding reaction can vary as a function of sequence. The sequence homology between the YB-1 CSD and the bacterial Csps amounts to about 40%. This is lower than that among the Csp's, where the sequence homology may be as high as 80%. Moreover, the YB-1 CSD and Csps differ in the length of their polypeptide chain. In YB-1 CSD, a four-residue insert is added to loop L_{34} and the N-terminus is extended by eight residues. The latter change lengthens the antiparallel β-sheet formed by $\beta 1$ and $\beta 4$ from the beta bulge formed by Lys^8 and Thr^7 onto Lys^3 in YB-1 CSD. The three N-terminal residues are not involved in β-sheet formation. These differences may lead to a situation where the rate-determining free energy barrier for the direct transition of D → F is higher than for the Csp's facilitating the collapse of the extended structures into partially folded structures in which the presence of native versus other contacts is (somewhat) unfavorable. Because interconversion between conformations is slower for compact than for extended states, such a situation may slow the formation of the native state (*37*). Sometimes the formation of a partially folded intermediate appears to be functional. A well-studied example is the Im7 protein, which forms an intermediate in which the hydrophobic residues Leu^{34} and Leu^{38} are exposed to the solvent in the native state, but more shielded in the intermediate (*38*). Whether for YB-1 CSD the formation of the partially folded intermediate is functional remains to be seen. It is interesting, however, that the central CSDs of the family of Y-box proteins are highly conserved, having 93% sequence identity. If these domains would give rise to partially folded intermediates they would clearly distinguish themselves from the bacterial Csp's and the intermediate might well be functional in the folding of the complete Y-box protein.

ACKNOWLEDGMENT

We gratefully acknowledge the contributions of S. Grzesiek to the early stages of YB-1 CSD studies and his gift of the YB1-CSD clone.

APPENDIX I

The analysis of the conventional T_1 experiments showed that the relaxation decays matched a monoexponential description. As delineated in Materials and Methods, the initial slope of the T_1-decay curves is equal to R_{1F} for the folded and R_{1U} for the unfolded form. This indicates that the effective relaxation rates will closely approach R_{1F} and R_{1U}, respectively. A more formal proof is outlined below.

Rephrasing eqs 3 and 4 we obtain:

$$M_{zF}(t) = \frac{M_{zF}(0)}{\lambda_1 - \lambda_2}[-(R_{1F} + \lambda_2)e^{\lambda_1 t} + (R_{1F} + \lambda_1)e^{\lambda_2 t}] \tag{A1.1}$$

and

$$M_{zU}(t) = \frac{M_{zU}(0)}{\lambda_1 - \lambda_2}[-(R_{1U} + \lambda_2)e^{\lambda_1 t} + (R_{1U} + \lambda_1)e^{\lambda_2 t}] \tag{A1.2}$$

for the folded and unfolded form, respectively.

If the decay is monoexponential the following equation is valid for the folded form:

$$\frac{M_{zF}(0)}{\lambda_1 - \lambda_2}[-(R_{1F} + \lambda_2)e^{\lambda_1 t} + (R_{1F} + \lambda_1)e^{\lambda_2 t}] = M_{zF}(0)e^{\lambda t} \tag{A1.3}$$

where λ is the effective relaxation time in the conventional T_1 experiment. This equation should hold at all times, including the regime in which the initial slope approximation applies. At this condition:

$$\frac{M_{zF}(0)}{\lambda_1 - \lambda_2}[-(R_{1F} + \lambda_2)(1 + \lambda_1 t) + (R_{1F} + \lambda_1)(1 + \lambda_2 t)] = M_{zF}(0)(1 + \lambda t) \tag{A1.4}$$

which leads to

$$1 - R_{1F}t = 1 + \lambda t \tag{A1.5}$$

meaning that:

$$\lambda = -R_{1F} \tag{A1.6}$$

The same result is obtained for the unfolded form, for which:

$$\lambda = -R_{1U} \tag{A1.7}$$

Thus, for the conditions prevailing in the experiments, exchange phenomena connected to the transition between the folded and unfolded forms have a negligible effect on the relaxation decays, which are determined by R_{1F} and R_{1U} respectively.

APPENDIX II

The observation of exchange cross-peaks between the signals of the unfolded and folded form of YB-1 CSD suggests a direct conversion between these two states. Such an interpretation implies that the unfolded form is an intermediate in the folding pathway of the CSD. This treatment of the data constitutes, however, the simplest approach and more complicated situations may occur which also give rise to the observed cross-peaks. Below we consider two folding pathways and examine the kinetics involved in the reaction schemes. The first is the so-called on-pathway, and the second is the so-called off-pathway, in which the residual structure of the unfolded form has to unfold before the native state can be formed. It is assumed that the steady state approximation is applicable to the completely unfolded state because its concentration is very low.

The On-Pathway Situation. This situation is characterized by the following reaction:

$$\mathbf{D} \underset{k_{DU}}{\overset{k_{UD}}{\rightleftharpoons}} \mathbf{U} \underset{k_{UF}}{\overset{k_{FU}}{\rightleftharpoons}} \mathbf{F}$$

with D, U, and F as described before. The rate equations describing the folding reaction are

$$\frac{d[D]}{dt} = -k_{DU}[D] + k_{UD}[U]$$

$$\frac{d[U]}{dt} = +k_{DU}[D] - (k_{UD} + k_{UF})[U] + k_{FU}[F] \tag{A2.1}$$

$$\frac{d[F]}{dt} = k_{UF}[U] - k_{FU}[F]$$

With the concentration of D in a steady-state situation we obtain:

$$\begin{aligned} \frac{d[U]}{dt} &= -k_{UF}[U] + k_{FU}[F] \\ \frac{d[F]}{dt} &= +k_{UF}[U] - k_{FU}[F] \end{aligned} \tag{A2.2}$$

Thus, in this situation the intensity of the exchange peaks is characterized by k_{UF} and k_{FU}.

The Off-Pathway Situation. To examine the likelihood of the unfolded form of YB-1 CSD being an off-pathway misfolded state we consider the reaction:

$$\mathbf{U} \underset{k_{UD}}{\overset{k_{DU}}{\rightleftharpoons}} \mathbf{D} \underset{k_{DF}}{\overset{k_{FD}}{\rightleftharpoons}} \mathbf{F}$$

Here the unfolded state, U, has to completely unfold to the (denatured) state D from which the native state, F, is obtained. The time dependence of the concentrations of the different forms of CSD are characterized by the rate equations:

$$\frac{d[U]}{dt} = -k_{UD}[U] + k_{DU}[D]$$

$$\frac{d[D]}{dt} = k_{UD}[U] - (k_{DU} + k_{DF})[D] + k_{FD}[F] \tag{A2.3}$$

$$\frac{d[F]}{dt} = k_{DF}[D] - k_{FD}[F]$$

For [D] in the steady-state condition we obtain:

$$\begin{aligned} \frac{d[U]}{dt} &= -\frac{k_{UD}k_{DF}}{k_{DU} + k_{DF}}[U] + \frac{k_{DU}k_{FD}}{k_{DU} + k_{DF}}[F] \\ \frac{d[F]}{dt} &= +\frac{k_{DF}k_{UD}}{k_{DU} + k_{DF}}[U] - \frac{k_{FD}k_{DU}}{k_{DU} + k_{DF}}[F] \end{aligned} \tag{A2.4}$$

Thus, the exchange rate constants characterizing the intensity of the exchange cross-peaks are now:

$$k_{UF} = \frac{k_{UD}k_{DF}}{k_{DU} + k_{DF}} \text{ and } k_{FU} = \frac{k_{DU}k_{FD}}{k_{DU} + k_{DF}} \tag{A2.5}$$

We consider the situation that the last step, D → F, conforms to the situation found for the small Csp's. Hence, we take $k_{DF} \approx 700\ s^{-1}$ and given the stability of the mesophilic proteins, $k_{FD} \approx 10\ s^{-1}$. In Figure 8 the values of k_{FU} as a function of the ratio k_{DF}/k_{DU} are compared with the experimental value of k_{FU}. It is clear that only at certain very specific conditions the off-pathway scheme may be consistent with the observations, i.e., for $k_{DF}/k_{DU} > 30$ and $k_{DF}/k_{DU} < 70$. Thus, when $k_{DU} \gg k_{DF}$ (left upper part of Figure 8) the unfolded form with residual structure is much more rapidly formed than the folded form, which is inconsistent with the experimental results. The same is true when $k_{DF} \gg k_{DU}$ (right lower part Figure 8), i.e., the folded form is much more rapidly formed than the unfolded form.

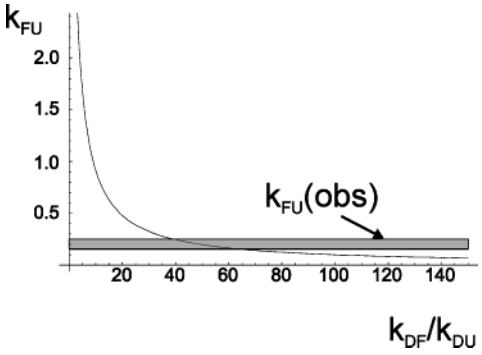

FIGURE 8: The rate constant for the conversion of the folded form (F) to the unfolded form (U) as a function of the ratio of the rate constants characterizing the conversion from the random coil form (D) to U and F. For the conditions at which the curve is obtained see text. The shaded area indicates the measured value of k_{FU} plus its estimated uncertainty.

REFERENCES

1. Palmer, A. G., III, Williams J., and McDermott A. (1996) Nuclear magnetic resonance studies of biopolymer dynamics, *J. Phys. Chem. 100,* 13293−13310.

2. Palmer, A. G., III (2001) NMR probes of molecular dynamics: overview and comparison with other techniques, *Annu. Rev. Biophys. Biomol. Struct. 30*, 129−155.
3. Lipari, G., and Szabo, A. (1982) Model-free approach to the interpretation of nuclear magnetic resonance relaxation in macromolecules. 1. Theory and range of validity, *J. Am. Chem. Soc. 104*, 4546−4559.
4. Lipari, G., and Szabo, A. (1982) Model-free approach to the interpretation of nuclear magnetic resonance relaxation in macromolecules. 2. Analysis of experimental results, *J. Am. Chem. Soc. 104*, 4559−4570.
5. Peng, J. W., and Wagner, G. (1992) Mapping of spectral density functions using heteronuclear NMR relaxation measurements, *J. Magn. Res. 98*, 308−332.
6. Farrow, N. A., Zhang, O., Szabo, A., Torchia, D. A., and Kay, L. E. (1995) Spectral density function mapping using ^{15}N-relaxation data exclusively, *J. Biomol. NMR 6*, 153−162.
7. Ishima, R., and Nagayama, K. (1995) Protein backbone dynamics revealed by quasi-spectral density function analysis of the amide N-15 nuclei, *Biochemistry 34*, 3162−3171.
8. Ishima, R., and Nagayama, K. (1995) Quasi-spectral-density mapping of $^{13}C^{\alpha}$-$^{1}H^{\alpha}$ vector dynamics using dipolar relaxation rates measured at several magnetic fields, *J. Magn. Reson., Ser. B 111*, 23−30.
9. Lefèvre, J.-F., Dayie, K. T., Peng, J. W., and Wagner, G. (1996) Internal mobility in the partially folded DNA binding and dimerisation domains of GAL-4: NMR analysis of the N−H spectral density functions, *Biochemistry 35*, 2674−2686.
10. Farrow, N. A., Zhang, O., Forman-Kay, J. D., and Kay, L. E. (1995) Comparison of the backbone dynamics of a folded and an unfolded SH3 domain existing in equilibrium in aqueous buffer, *Biochemistry 34*, 868−878.
11. Farrow, N. A., Zhang, O., Forman-Kay, J. D., and Kay, L. (1997) Characterization of the backbone dynamics of folded and denatured states of an SH3 domain, *Biochemistry 36*, 2390−2402.
12. Alexandrescu, A. T., and Shortle, D. (1994) Backbone dynamics of a highly disordered 131 residue fragment of staphylococcal nuclease, *J. Mol. Biol. 242*, 527−546.
13. Zhang, O., Kay, L. E., Shortle, D., and Forman-Kay, J. D. (1997) Comprehensive NOE characterization of a partially folded large fragment of Staphylococcal nuclease Δ131Δ, using NMR methods with improved resolution, *J. Mol. Biol. 272*, 9−20.
14. Vugmeyster, L., Kroenke, C. D., Picart, F., Palmer, A. G., III, and Raleigh, D. P. (2000) ^{15}N $R_{1\rho}$ measurements allow the determination of ultrafast protein folding rates, *J. Am. Chem. Soc. 122*, 5387−5388.
15. Kloks, C. P. A. M., Spronk, C. A. E. M., Lasonder, E., Hoffmann, A., Vuister, G. W., Grzesiek, S., and Hilbers, C. W. (2002) The solution structure and DNA binding properties of the cold shock domain of the human Y-box protein YB-1, *J. Mol. Biol. 316*, 317−326.
16. Murzin, A. G. (1993) OB (oligonucleotide/oligosaccharide binding)-fold: common structural and functional solution for non-homologous sequences, *EMBO J. 12*, 861−867.
17. Kloks, C. P. A. M., Hoffmann, A., Omichinski, J. G., Vuister, G. W., Hilbers, C. W., and Grzesiek, S. (1998) Resonance Assignment and secondary structure of the cold shock domain of the human YB-1 protein, *J. Biomol. NMR 12*, 463−464.
18. Delaglio, F., Grzesiek, S., Vuister, G. W., Zhu, G., Pfeifer, J., and Bax, A. (1995) NMRPipe: A multidimensional spectral processing system based on UNIX pipes, *J. Biomol. NMR 6*, 277−293.
19. Garrett, D. S., Powers, R., Gronenborn, A. M., and Clore, G. M (1991) A common sense approach to peak-picking in two-, three-, and four-dimensional spectra using automatic computer analysis of contour diagrams, *J. Magn. Reson. 95*, 214−220.
20. Wider, G., Neri, D., and Wüthrich, K. (1991) Studies of slow conformational equilibria in macromolecules by exchange of heteronuclear longitudinal 2-spin-order in a 2D difference correlation experiment, *J. Biomol. NMR 1*, 93−98.
21. Farrow, N. A., Zhang, O., Forman-Kay, J. D., and Kay, L. E. (1994) A heteronuclear correlation experiment for simultaneous determination of ^{15}N longitudinal decay and chemical exchange rates of systems in slow equilibrium, *J. Biomol. NMR 4*, 727−734.
22. Fushman, D., Weisemann, R., Thüringer, H., and Rüterjans, H. (1994) Backbone dynamics of ribonuclease T1 and its complex with 2′GMP studied by two-dimensional heteronuclear NMR spectroscopy, *J. Biomol. NMR 4*, 61−78.
23. Izumi, H., Imamura, T., Nagatani, G., Ise, T., Murakami, T., Uramoto, H., Torigoe, T., Ishiguchi, H., Yoshida, Y., Nomoto, M., Okomoto, T., Uchiumi, T., Kuwano, M., Funa, K., and Kohno, K. (2001) Y box-binding protein-1 binds preferentially to single-stranded nucleic acids and exhibits 3′-5′ exonuclease activity, *Nucleic Acids Res. 29*, 1200−1207.
24. Feng, W., Tejero, R., Zimmerman, D. E., Inouye, M., and Montelione, G. T. (1998) Solution NMR structure and backbone dynamics of the major cold-shock protein (CspA) from *Escherichia coli*: evidence for conformational dynamics in the single-stranded RNA-binding site, *Biochemistry 37*, 10881−10896.
25. Rietman, B. H., Folkers, P. J. M., Folmer, R. H. A., Tesser, G. I., and Hilbers, C. W. (1996) The solution structure of the synthetic circular peptide CGVSRQGKPYC: NMR studies of the folding of a synthetic model for the DNA-binding loop of the ssDNA-binding protein encoded by gene V of phage M13, *Eur. J. Biochem. 238*, 706−713.
26. Larson, G., Martinez, G., Schleucher, J., and Wijmenga, S. S. (2003) Detection of nano-second internal motion and determination of overall tumbling times independent of the time scale of internal motion in proteins from NMR relaxation data, *J. Biomol. NMR, 27*, 291−312.
27. Schwalbe, H., Fiebig, K. M., Buck, M., Jones, J. A., Grimshaw, S. B., Spencer, A., Glaser, S. J., Smith, L. J., and Dobson, C. M. (1997) Structural and dynamical properties of a denatured protein. Heteronuclear 3D NMR experiments and theoretical simulations of lysozyme in 8 M urea, *Biochemistry 36*, 8977−8991.
28. Klein-Seetharaman, J., Oikawa, M., Grimshaw, S. B., Wirmer, J., Duchardt, E., Ueda, T., Imoto, T., Smith, L. J., Dobson, C. M., and Schwalbe, H. (2002) Long-range interactions within a non-native protein, *Science 295*, 1719−1722.
29. Reid, K. L., Rodriguez, H. M., Hillier, B. J., and Gregoret, L. M. (1998) Stability of folding properties of a model β-sheet protein, *Escherichia coli* CspA. *Protein Sci. 7*, 470−479.
30. Mueller, U., Perl, D., Schmid, F. X., and Heinemann, U. (2000) Thermal stability and atomic-resolution crystal structure of the *Bacillus caldolyticus* cold shock protein, *J. Mol. Biol. 297*, 295−988.
31. Perl, D., Welker, C., Schindler, T., Schröder, K., Marahiel, M. A., Jaenicke, R., and Schmid, F. X. (1998) Conservation of rapid two-state folding in mesophilic, thermophilic and hyperthermophilic cold shock proteins, *Nat. Struct. Biol. 5*, 229−235.
32. Schindler, T., and Schmid, F. X. (1996) Thermodynamic properties of an extremely rapid protein folding reaction, *Biochemistry 35*, 16833−16842.
33. Perl, D., Mueller, U., Heinemann, U., and Schmid, F. X. (2000) Two exposed amino acid residues confer thermostability on a cold shock protein, *Nat. Struct. Biol. 7*, 380−383.
34. Zeeb, M., Jacob, M. H., Schindler, T., and Balbach, J. (2003), ^{15}N relaxation study of the cold shock protein CspB at various solvent viscosities, *J. Biomol. NMR. 27*, 221−234.
35. Kremer, W., Schuler, B., Harrieder, S., Geyer, M., Gronwald, W., Welker, C., Jaenicke, R., and Kalbitzer, H. R. (2001) Solution NMR structure of the cold-shock protein from the hyperthermophilic bacterium *Thermotoga maritima*, *Eur. J. Biochem. 268*, 2527−2539.
36. Gunasekaran, K., Eyles, S. J., Hagler, A. T., and Gierasch, L. M. (2001) Keeping it in the family: folding studies of related proteins, *Curr. Opin. Struct. Biol. 11*, 83−93.
37. Dinner, A. R., Šali, A., Smith, L. J., Dobson, C. M., and Karplus, M. (2000) Understanding protein folding via free-energy surfaces from theory and experiment, *Trends Biochem. Sci*. 331−339.
38. Capaldi, A. P., Kleanthous, C., and Radford, S. E. (2002) Im7-folding mechanism: misfolding on a path to the native state, *Nat. Struct. Biol. 9*, 209−216.
39. Konradi, R., Billeter, M., and Wüthrich, K. (1996) MOLMOL: a program for display and analysis of macromolecular structures, *J. Mol. Graphics 14*, 51−55.

BI049524S